Journal of Hazardous Materials 194 (2011) 407–413

Contents lists available at ScienceDirect

Journal of Hazardous Materials

journal homepage: www.elsevier.com/locate/jhazmat

Nano-lead particle synthesis from waste cathode ray-tube funnel glass

Mingfei Xing, Fu-Shen Zhang*

Research Center for Eco-Environmental Sciences, Chinese Academy of Sciences, 18 Shuangqing Road, Beijing 100085, China

ARTICLE INFO

Article history:
Received 18 April 2011
Received in revised form 3 August 2011
Accepted 3 August 2011
Available online 9 August 2011

Keywords:
Hazardous waste
CRT
Lead
Inert-gas consolidation
Nanoparticle

ABSTRACT

Waste cathode ray-tube (CRT) funnel glass is classified as hazardous waste since it contains high amount of lead. In the present study, a novel process for lead nanopowder synthesis from this type of glass was developed by combining vacuum carbon–thermal reduction and inert-gas consolidation procedures. The key trait of the process was to evaporate lead out of the glass to obtain harmless glass powder and synchronously produce lead nanoparticles. In the synthesis process, lead oxide in the funnel glass was firstly reduced to elemental lead, and evaporated rapidly in vacuum circumstance, then quenched and formed nano-size particles on the surface of the cooling device. Experimental results showed that temperature, pressure and argon gas flow rate were the major parameters controlling lead evaporation ratio and the morphology of lead nanoparticles. The maximum lead evaporation ratio was 96.8% and particles of 4–34 nm were successfully obtained by controlling the temperature, holding time, process pressure, argon gas flow rate at 1000 °C, 2–4 h, 500–2000 Pa, 50–200 ml/min, respectively. Toxicity characteristic leaching procedure (TCLP) results showed that lead leaching from the residue glass met the USEPA threshold. Accordingly, this study developed a practical and environmental-friendly process for detoxification and reclamation of waste lead-containing glass.

1. Introduction

Cathode ray-tube (CRT) is an important device mainly used as video display component in television and computer and it will eventually be replaced by advanced display technology [1], which will result in a huge number of waste CRTs. CRT funnel glass generally contains high level of PbO (20–30%) [2], which may contaminate our living environment by leaching of lead ions from broken lead containing glass when mixed with acid waters in waste landfills [3,4]. It is difficult for the conventional acid leaching methods to extract lead completely from the funnel glass due to its special stable structure [5–7]. Therefore, some pretreatments were developed to improve the lead extraction efficiency by breaking the glass's structure, such as wet ball-milling treatment, ultrasonically enhanced leaching and subcritical water treatment [8–10]. However, there were still some disadvantages among these methods, e.g., long process time, high-energy consumption and low lead recovery efficiency. All of these factors limit of the recycling of waste CRT.

Metal nanoparticles have been extensively used in a variety of research fields due to their novel electromagnetic, chemical, thermal and optical properties [11]. Lead nanopowder is one important nano-material that has a great potential to be used as negative electrode materials in lithium-ion batteries, high-energy radiation protection composites, catalysts, wavelength filters, and superconducting materials [12–16]. Currently several methods have been developed for the preparation of nano-sized materials, e.g., solution-phase chemical reduction, pulsed laser deposition, chemical vapor deposition, gas-phase condensation and mechanical milling [17–22]. Among these methods, inert-gas consolidation (IGC) method has become an attractive research area as it produces nanoparticles in large scale and is characterized by more energy-effective, environmentally friendly, and easier to produce products of preferred nanoparticles than the traditional wet chemistry route [23]. Therefore, a great number of researches have been carried out on IGC method of which the main raw materials usually are high purity metal, e.g., Cu, Pd, Fe, Al [24–26]. However, there are few reports about using waste electrical and electronic equipments (WEEE), which contain high levels of metals as raw materials of IGC method to produce nanopowder. The local structure around lead can be changed by reacting with some reducing agents such as AlN, TiN, SiC and H_2, and the reducing reaction can help extract lead from CRT glass [27–30]. In previous works, we found lead can be extracted from CRT funnel glass efficiently by a pyro-vacuum process [31]. It attributed to vitreous lead oxides changing to metallic lead by carbon powder and the lower boiling point of metallic lead at vacuum condition. Furthermore, in our recent study, lead nanoparticles were successful prepared by retrofitting the pyro-vacuum process and the lead-containing glass was also converted into harmless glass. As mentioned above, the

* Corresponding author. Tel.: +86 10 62849515; fax: +86 10 62849515.
E-mail address: fszhang@rcees.ac.cn (F.-S. Zhang).

0304-3894/$ – see front matter © 2011 Elsevier B.V. All rights reserved.
doi:10.1016/j.jhazmat.2011.08.003

Table 1
Chemical composition of the investigated funnel glass by X-ray fluorescence (XRF).

Elements	wt%
SiO_2	52.5 ± 0.37
PbO	22.9 ± 0.21
K_2O	8.66 ± 0.07
Na_2O	5.67 ± 0.05
Al_2O_3	3.68 ± 0.05
CaO	2.74 ± 0.03
MgO	2.43 ± 0.03
Fe_2O_3	0.57 ± 0.03
SrO	0.16 ± 0.01
BaO	0.11 ± 0.01
P_2O_5	0.04 ± 0.01
ZnO	0.01 ± 0.001

vacuum carbon–thermal reduction method and the inert-gas consolidation method were combined together and formed a new one-step preparation of lead nanoparticles which using the waste CRT glass as lead source.

The aims of this study were to: (1) examine the effect of various experimental factors on lead evaporate ratio in low pressure environment of argon gas; (2) study the main influence factors of the nanoparticles morphology and size; (3) optimize the experimental parameters base on the consideration of lead evaporation ratio, nanoparticle morphology and the environmental security of the residues.

2. Materials and methods

2.1. Sample preparation

The CRT funnel glass, provided by Huaxing Environmental Protection Corporation (China), was first broken into small pieces (≤10 mm) and coatings on the surface of the glass were removed by wet scrubbing and ultrasonic cleaning methods [32]. Afterward, the CRT glass particles were dry ball milled and sieved through a 200-mesh sieve (≤74 μm), and then the powder was dry at 105 °C for 24 h. Chemical composition of the glass powder was examined by X-ray fluorescence (XRF), and the results were presented in Table 1. Other materials used in the experiments were all analytical reagents unless otherwise mentioned.

2.2. Experimental procedure

Fig. 1 shows a schematic diagram of the setup used for the production of lead nanoparticles. The installation consists of four basic units, i.e., heating system (1–3), water cooling system (6 and 7), vacuum system (8–10) and argon gas supply system (11 and 12). The milled CRT glass powder (5 g) was mixed with 10% carbon powder and loaded in the quartz boat which was then placed in the process chamber (length 700 mm, inner diameter 50 mm). All connections were made with vacuum flanges to allow gas tight operation at subatmospheric pressures. The chamber was closed air-tight, evacuated by a vacuum pump to a pressure less than 1000 Pa. Then high purity argon gas (99.999% purity) was blown to the chamber to remove the air in the system. This procedure was repeated three times to ensure a pure argon gas environment. Then the mixed powder was heated by graphite heaters to the set temperature. After the set temperature was reached, water cooling valve was opened, and argon gas flow rate and system pressure were adjusted to the operating conditions. The pressure in the chamber was measured by a pressure gauge and controlled by a vacuum valve. The argon gas flow rate was measured by a flow meter and controlled by a valve under vacuum condition. In addition, the quartz chamber could form cracks on its surface that might shorten its lifespan if the temperature was above 1100 °C. Therefore, the highest temperature was limited at 1100 °C in this study.

In this study, the examined temperatures were 600, 700, 800, 900, 1000 and 1100 °C, holding times were 1, 2, 3 and 4 h, system pressures were 500, 1000, 2000 and 4000 Pa, argon gas flow rates were 0, 50, 100 and 200 ml/min, respectively. When each treatment was finished, the process chamber was slowly cooled down to room temperature. The residue together with the black Pb nanopowder on the water cooling system were collected, dried and stored in a desiccator for further analysis.

2.3. Analysis

The nanopowder and the residues were digested by HNO_3–$HClO_4$–HF [33] and examined by inductively coupled plasma optical emission spectrometer (ICP-OES, OPTIMA 2000). Lead evaporation ratios were calculated according to the lead content before and after the treatment. Lead leaching behavior of the residues was evaluated according to the toxicity characteristic leaching procedure (TCLP) of USEPA [34]. All the experiments were duplicated and only the mean values were reported. The measurement errors were around ±1%.

The collected nanopowder was characterized by X-ray diffraction (XRD) using the Ni-filtered Cu Kα radiation on a RigakuD/MAX2500 diffractometer over an angle of $10° < 2\theta < 80°$. Then the nanopowder were withstood ultrasonic dispersion treatment in ethanol for 30 min and transmission electron microscopy (TEM, H7500) was employed to examine the size and morphology of the nanoparticles.

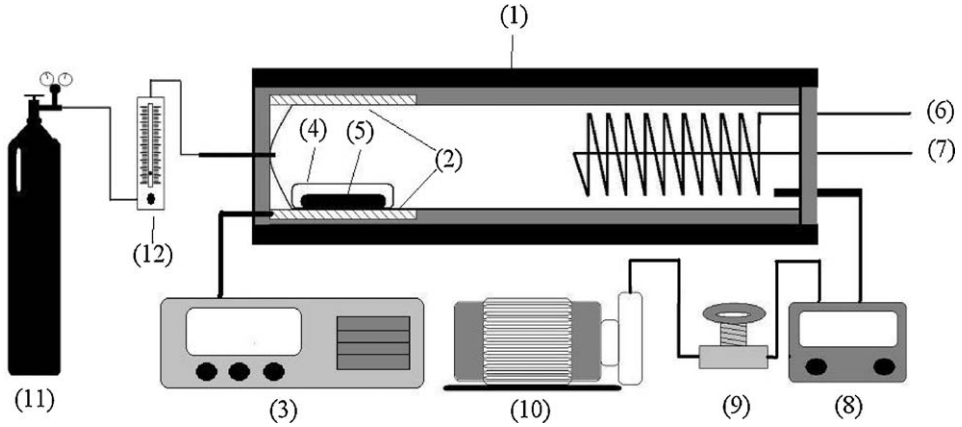

Fig. 1. Schematic diagram of lead nanoparticles fabrication installation. (1) Process chamber (2) graphite heaters (3) temperature control device (4) quartz boat (5) pretreated CRT powder (6 and 7) inlet and outlet of water cooling device (8) vacuum gauge (9) vacuum valve (10) vacuum pump (11) argon gas installation (12) flow meter.

3. Results and discussion

3.1. Effects of various parameters on lead evaporation ratio

Lead in funnel glass mainly exists in the form of lead oxide and the melting point of lead oxide (melting point 888 °C, boiling point 1535 °C) is much higher than lead (melting point 328 °C, boiling point 1740 °C) under normal condition [35]. It is difficult to evaporate lead oxide from funnel glass at a low temperature, thus carbon powder (particle size < 74 μm) is used as a reducing agent to reduce lead oxide into metallic lead to increase the evaporation velocity. According to literature [28], plenty of metallic lead can be assembled on the surface of CRT glass after the reducing reaction, and the higher was the temperature of reaction, the lower was the lead content inside the glass powder. Therefore, temperature is a key factor for both lead oxide reduction velocity and metallic lead evaporation velocity. Lead oxide can be reduced to lead under normal pressure when the temperature is higher than 580 °C according to the carbon–thermal reduction of lead oxide [36], and the reduction rate of lead oxide is increased rapidly with the increase of temperature. Meanwhile lead evaporation velocity increases rapidly with an increase in the temperature. When the system pressure maintained at 10 Pa and the temperature increased from 800 °C to 1000 °C, corresponding the lead evaporation velocity increased from 0.4×10^{-3} g cm^{-2} s^{-1} to 6.6×10^{-3} g cm^{-2} s^{-1} [35].

Fig. 2(a) shows that lead evaporation ratio increased quickly with the increase of temperature below 900 °C. Lead evaporation ratio was only about 30.8% at 600 °C and rapidly increased to 93.8% at 900 °C. Then the growth of lead evaporation ratio slowed down and lead evaporation ratio reached its maximum of 96.3% at 1100 °C. In addition, the quartz chamber could form cracks on its surface which might shorten its lifespan if the temperature was above 1100 °C, and moreover lead evaporation ratio was 96.1% at 1000 °C and it was only 0.2% less than 1100 °C. Therefore, the highest temperature was limited at 1000 °C in this study.

Fig. 2(b) indicates that lead evaporation ratio increased with the increase of holding time and increased fast in the first 2 h (95.9%). When the holding time was more than 2 h, lead evaporation ratio increased slowly and reached its maximum at 4 h (96.1%). Therefore, the optimum holding time was 2 h with temperature, pressure and argon gas flow rate were fixed at 1000 °C, 500 Pa and 50 ml/min, respectively.

Fig. 2(c) shows the effect of argon gas flow rate on lead evaporation ratio. Lead evaporation ratio increased rapidly with the increase of argon gas flow rate below 50 ml/min, e.g., increased from 94.3% at 0 ml/min to 96.1% at 50 ml/min. Then lead evaporation ratio increased slowly and reached its maximum at 96.8% when the gas flow rate was 200 ml/min. Argon gas in the synthesis process acted as a driving force to blow the lead vapor out from the CRT glass powder, so lead evaporation ratio can be increased by increasing argon gas flow rate.

System pressure plays an important role in lead evaporation velocity. Fig. 2(d) illustrates that lead evaporation ratios at different pressures when temperature, argon gas flow rate and holding time were fixed at 1000 °C, 50 ml/min and 4 h respectively. The lower was the system pressure; the higher was the velocity of lead evaporation. Meanwhile, lower pressure means higher moving speed of argon gas in chamber if at the same flow rate condition, and lead can be quickly blown out from the surface of CRT glass powder. Therefore, lead evaporation ratio kept on decreasing with the increase of system pressure. Generally, lead evaporation ratios were >92% when the pressure was lower than 2000 Pa. Lead evaporation ratio

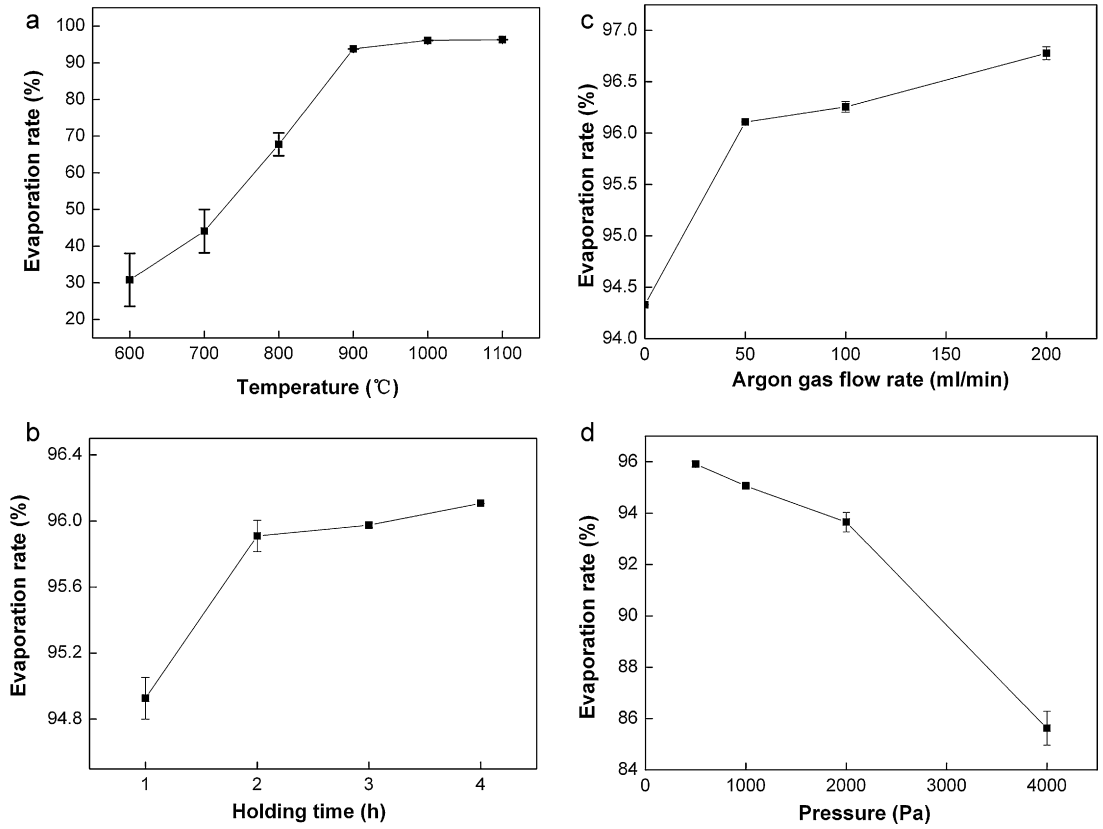

Fig. 2. Effects of various parameters on lead evaporation ratio. (a) Effect of temperature on lead evaporation ratio (pressure = 500 Pa, argon gas flow rate = 50 ml/min, holding time = 4 h). (b) Effect of holding time on lead evaporation ratio (temperature = 1000 °C, pressure = 500 Pa, argon gas flow rate = 50 ml/min). (c) Effect of argon gas flow rate on lead evaporation ratio (temperature = 1000 °C, pressure = 500 Pa, holding time = 4 h). (d) Effect of system pressure on lead evaporation ratio (temperature = 1000 °C, argon gas flow rate = 50 ml/min, holding time = 4 h).

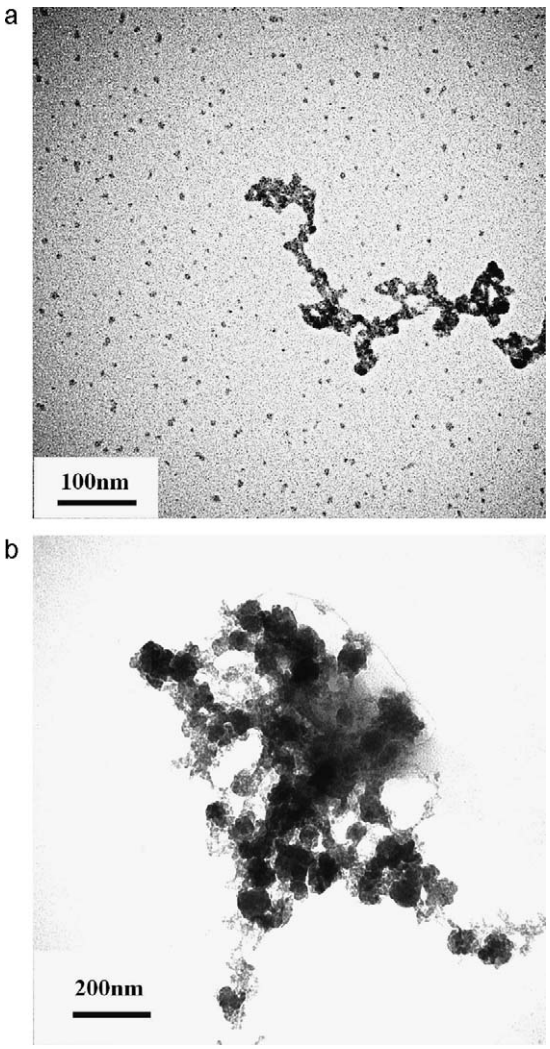

Fig. 3. TEM pictures of lead nanoparticles prepared at different temperatures (argon gas flow rate = 50 ml/min, system pressure = 500 Pa, holding time = 4 h, (a) temperature = 1000 °C; (b) temperature = 1100 °C).

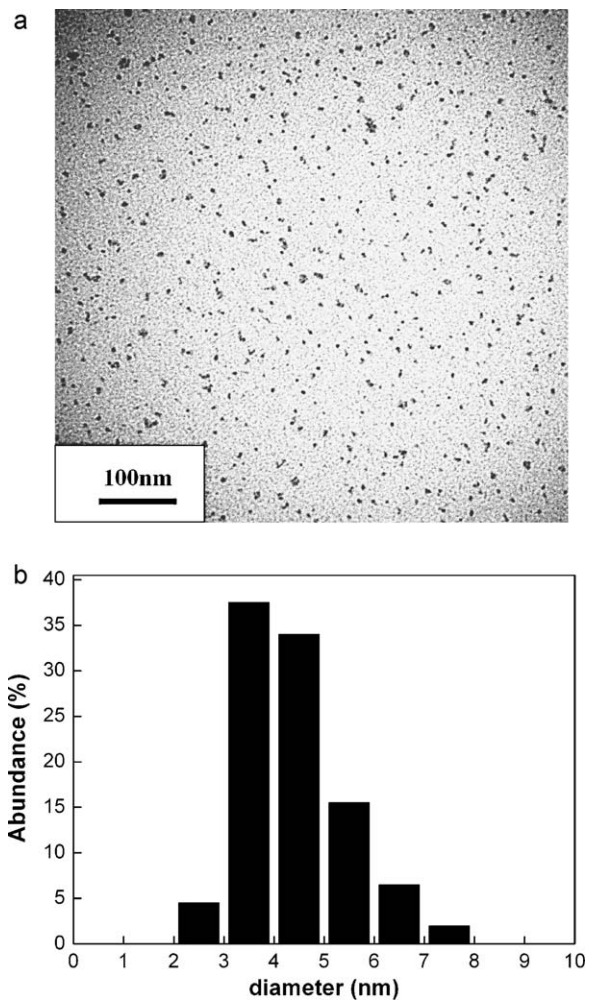

Fig. 4. TEM picture and particle size distribution of lead nanoparticles (temperature = 1000 °C, argon gas flow rate = 200 ml/min, system pressure = 500 Pa, holding time = 4 h).

decreased sharply from 93.7% at 2000 Pa to 85.6% at 4000 Pa when the system pressure was higher than 2000 Pa.

In addition, the particle size of CRT glass also played an important role in lead evaporation ratio. If the particles were too large, only a small part of the lead oxide on the CRT particles' surface will be reduced into metallic lead and the lead that around the centre of the particles cannot be evaporated will be left in the residues. However, in actual application, the smaller were the particles, the larger was the energy consumption. In this paper, the CRT glass was ball-milled smaller than 74 μm in order to obtain high lead evaporation ratio without considering the energy consumption. The experimental results show that these small particles can be well mixed with carbon powder and the lead can be easily evaporated from these small particles.

3.2. Effects of various parameters on nanoparticle morphology

Temperature plays an important role on the size and morphology of the nanoparticles. Fig. 3(a) shows that the TEM picture of Pb nanoparticles obtained at 1000 °C, 500 Pa, 50 ml/min and maintained 4 h, respectively. It appears that most of the Pb particles were evenly dispersed, and only a small part of the particles were stuck together. The nanoparticles' sizes range from 3 nm to 11 nm with an average diameter of 7 nm. Fig. 3(b) shows that the TEM picture of Pb nanoparticles produced at 1100 °C while other experimental conditions remained the same as Fig. 3(a). The particles size range from 55 nm to 120 nm with an average diameter of 80 nm. The TEM picture shows that the average particle size of Fig. 3(b) was much bigger than Fig. 3(a) and most of the produced particles were stuck together in cluster and formed agglomerate, which were generally irregular in shape.

According to previous reports [37,23], nanoparticle synthesis based on inert-gas consolidation has common mechanisms involving precursor gas reaction, surface growth, particle nucleation, coagulation and coalescence. However, the finally produced agglomerate characteristics depend mainly on the competition between coagulation and coalescence. Once particles form in the gas phase, they coagulate at a rate that is proportional to the square of their number concentration and that is only weakly dependent on particle size. And the density of particles within the gas phase increases as the temperature is increased result in higher the collision frequency of the particles, such as coalescence occurs more frequently. Generally, at lower temperatures, where coalescence is negligibly slow, loose agglomerates with quite open structures and partially sintered non-spherical particles are formed. At sufficiently high temperatures, particles coalesce faster than they coagulate, and spherical particles could be produced [38].

Fig. 4 shows the TEM picture and particle size distribution of the prepared nanoparticles when temperature, argon gas flow rate,

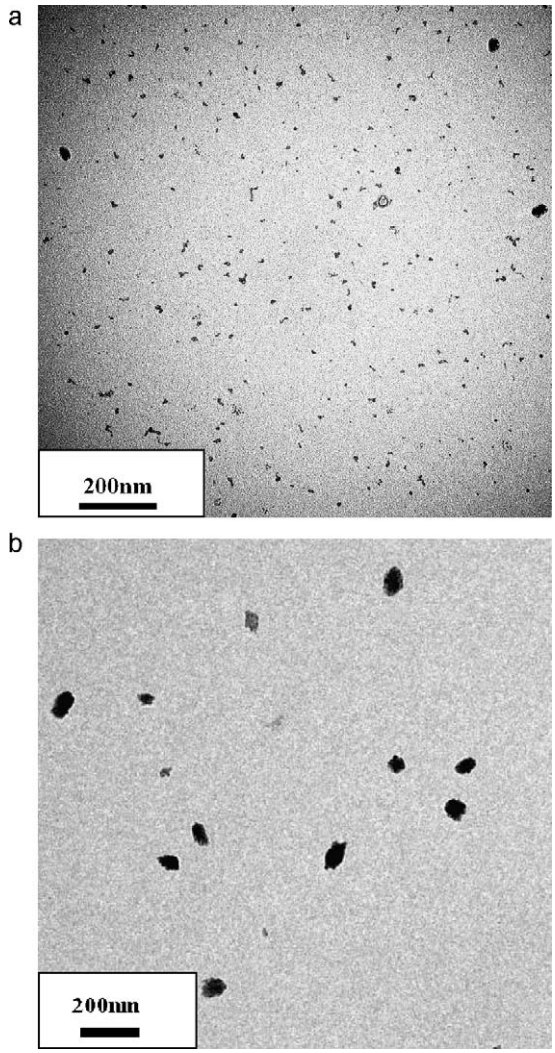

Fig. 5. TEM pictures of lead nanoparticles prepared at different pressures (temperature = 1000 °C, holding time = 4 h, argon gas flow rate = 50 ml/min, (a) system pressure = 1000 Pa; (b) system pressure = 4000 Pa).

system pressure and holding time were 1000 °C, 200 ml/min, 500 Pa and 4 h respectively. All the particles were evenly dispersed and the agglomeration disappeared when the gas flow rate was increased from 50 ml/l to 200 ml/min by comparing Fig. 3(a) and Fig. 4(a). The comparison illustrates that increasing the gas flow rate can reduce the degree of agglomeration of the nanoparticles. The TEM result indicated that within a certain range, increasing the argon gas flow rate can improve the dispersion effect of the nanoparticles and more tiny nanoparticles were obtained. This could be explained by the following two facts: (1) raising the argon gas flow rate can increase the collision efficiency between lead vapor and argon gas to improve the quenching effect; (2) the argon gas acted as a driving force which blew the lead vapor from the hot evaporation zone to the water cooling zone, resulted in a reduction of residence time of the nuclei to further improve the quenching effect [39]. Therefore, Fig. 4(b) shows a narrow particle size distribution range from 2 nm to 8 nm when the argon gas flow rate was 200 ml/min. And the primary particles size of 3–5 nm in diameter account for 71% with the average diameter is 4 nm. So the argon gas flow rate plays an important role on the morphology of the nanoparticles.

System pressure, which affects the morphology of nanoparticles greatly, is another key point to the size of the nanoparticles. Fig. 5 indicates the effect of system pressure on the mean size of the nanoparticles when the other experimental conditions were

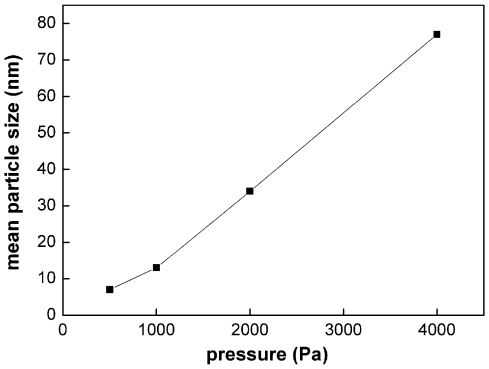

Fig. 6. Particle sizes of lead nanoparticles prepared at different pressures (temperature = 1000 °C, holding time = 4 h, argon gas flow rate = 50 ml/min).

fixed at 1000 °C, 50 ml/min and 2 h. Fig. 6 shows the mean size of the prepared nanoparticles increased with the increase of system pressure, e.g., increased from 7 nm at 500 Pa to 77 nm at 4000 Pa. The reason is that lowering the pressure increases vapor dispersion and dilution, therefore lowering the volume concentration of particulate materials produced by condensation and slowing their growth by coagulation so small particles were obtained. But at the higher pressures the coagulation rate is improved which leading to faster growth of the nucleuses and larger particles were formed [40]. Therefore, unlike temperature and system pressure, argon gas flow rate has a different effect on the morphology of nanoparticles, that is, increasing the argon gas flow rate can decrease the average size of nanoparticles.

3.3. Properties of lead nanoparticles

After the treatment, the process chamber was opened and the lead nanopowder was collected and quickly preserved in ethanol to prevent congregation and oxidation. In this study, the system pressure ranged from 500 Pa to 4000 Pa, which was high for a vacuum. These vacuum conditions may contain a very low level of oxygen that could affect the final product composition. However, argon gas was continuously pumped into the processing chamber to remove the oxygen during the nanoparticles synthesis process and the oxygen content in the chamber was very low. The argon gas was not only acted as a quench gas, but also as an inert gas that prevents the metallic lead nanoparticles to be oxidized. Therefore, the main obtained nanoparticles were metallic lead before the chamber was opened. However, limited by the experimental conditions, some of the Pb nanoparticles were oxidized into PbO for their high activity when they were exposed in an aerobic environment during the collecting process. Thus, the lead oxide was mainly formed in the collecting process, which should be improved to be operated in anaerobic conditions to avoid the oxidation of metallic lead. Fig. 7 shows the X-ray diffraction patterns of the prepared lead nanopowder at different conditions. Fig. 7(a) (0 ml/min, 1000 °C, 500 Pa, 4 h) indicates that the peaks were sharp and the background signal was low indicating well-ordered crystalline materials. Most of the peaks in the patterns can be indexed by the known patterns of pure Pb metal (PDF card #65-2873), and only a few distinct peak of lead oxide (PDF card #38-1477) and lead sulfides (PDF card #05-0592) were visible. The elemental sulfur may come from the carbon powder. But more lead oxide peaks were visible in Fig. 7(b) (50 ml/min, 1000 °C, 500 Pa, 4 h) and the full width at half-maximum intensity of the XRD peak of Fig. 7(b) was larger than Fig. 7(a) which meant that the average particle size of Fig. 7(b) was smaller than that of Fig. 7(a) according to Scherrer's formula. Therefore, the XRD results showed the same variation trend with TEM observations

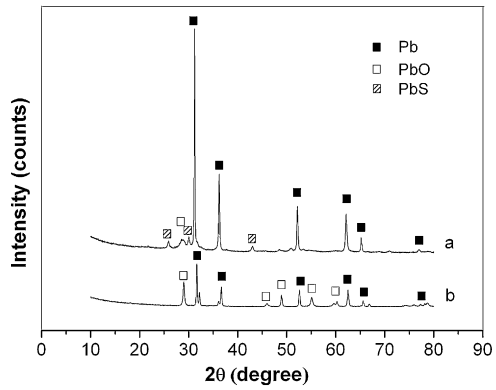

Fig. 7. X-ray diffraction patterns of lead nanopowder (temperature = 1000 °C, pressure = 500 Pa, holding time = 4 h, (a) argon gas flow rate = 0 ml/min; (b) argon gas flow rate = 50 ml/min).

Table 2
Chemical composition of lead nanoparticles by ICP-OES.

Elements	wt%
Pb	95.09 ± 0.15
Na	2.80 ± 0.09
K	1.30 ± 0.03
Ti	0.56 ± 0.03
Mg	0.11 ± 0.01
Al	0.06 ± 0.01

that increasing the argon gas flow rate can decrease the average size of nanoparticles.

$$D = \frac{K\lambda}{\beta \cos\theta}$$

In the formula, D is the grain size, K is the crystallite-shape factor, (is the X-ray wavelength, β is the full width at half-maximum intensity of the XRD peak and (is the diffraction angle. The crystallite-shape factor mainly depends on the shape of the particle. The value of K is often between 0.89 and 0.94 (spherical particle K = 0.89, cube particle K = 0.94). In this paper, the obtained nanoparticles were spherical, thus 0.89 was chosen as the crystallite-shape factor. The XRD results reflect that the smaller size of the nanoparticles, the larger surface area they have and the easier the nanoparticles to be oxidized. To further understand the chemical composition of the production, the nanopowder (50 ml/min, 1000 °C, 500 Pa, 4 h) was analyzed by ICP-OES and the results were shown in Table 2. It can be seen that the main element in the prepared nanopowder was metallic lead, which accounted for 95.09%. A small portion of other elements, which was also evaporated from the CRT glass, was mainly Na (2.80%), K (1.30%), Ti (0.56%), Mg (0.11%) and Al (0.06%).

3.4. Properties of the residues

Most residues after the treatment were in powder form, while some residues were in porous form. The forms of the residues mainly depend on the amount of the carbon powder (melting point 3727 °C). The melting point of the CRT glass is low and it can be completely melted together above 600 °C when the amount of carbon powder less than 5%. However, when the adding amount was more than 5%, more carbon powder was left in the residues, which can prevent the CRT glass powder from melting together. Meanwhile, the residues in powder form will help increase the lead evaporation ratio. The weight and the lead content of the residues decreased with the increase of temperature, holding time, but system pressure was on the contrary. Under the optimum experimental conditions (1000 °C, 2–4 h, 500–2000 Pa and 50–200 ml/min), the amount of the residues ranged from 3.47 g to 3.81 g and the lead content of the residues ranged from 0.91% to 1.72%.

TCLP method was performed to evaluate the safety of the residues. Table 3 presents the lead concentrations in the leachates of all residues after the treatments. Generally speaking, lead concentration decreased with the increase of temperature and holding time, but system pressure was on the contrary. The content of PbO in untreated CRT particles was high (22.9%) and there were plenty of cracks on these particles' surface, which were formed during the dry-ball milled. The lead oxide on the particles' surface can be leached by the leaching agent. Therefore, the leaching concentration of untreated CRT glass was 363.3 mg/l and it was much higher than the TCLP lead threshold (5 mg/l), which demonstrated the CRT glass was a typical hazardous waste. However, when the temperature was higher than 1000 °C and the system pressure was lower than 2000 Pa, all the leaching concentrations were lower than 5.0 mg/l and met the TCLP lead threshold. After the treatment, most of the PbO were evaporated from the CRT particles. The surface of the particles was melted and the rough surface was changed to smooth surface while the residues were still powders. Thus, the lead atoms left in the residues were firmly fixed again by encapsulation in the cavity of the glass network and the lead extraction cannot be fulfilled under normal conditions [8]. In addition, among the leaching results, leaching concentrations were more than 2000 mg/l when the temperature was below 800 °C and it was much higher than untreated CRT glass. This phenomenon confirms that the stable structure of CRT glass can be completely broken by heating that result in the lead can be easily evaporated from the glass particles to fulfill the purpose of detoxification of the waste CRT funnel glass.

Table 3
TCLP results for lead of the residue glasses.

Temperature(°C)	Pressure(Pa)	Holding time(h)	Argon gas flow rate(ml/min)	TCLP results (mg/L)
600	500	4	50	2155.00 ± 30.00
700	500	4	50	2458.00 ± 56.00
800	500	4	50	2102.40 ± 16.70
900	500	4	50	30.34 ± 1.55
1000	500	4	50	0.31 ± 0.01
1100	500	4	50	0.33 ± 0.01
1000	500	1	50	0.92 ± 0.01
1000	500	2	50	0.58 ± 0.04
1000	500	3	50	0.55 ± 0.01
1000	500	4	0	0.89 ± 0.03
1000	500	4	100	2.62 ± 0.09
1000	500	4	200	1.22 ± 0.05
1000	1000	4	50	1.03 ± 0.06
1000	2000	4	50	3.45 ± 0.05
1000	4000	4	50	60.76 ± 1.17

4. Conclusions

Vacuum carbon–thermal reduction combined with inert-gas consolidation process was an effective approach for waste CRT funnel glass detoxification and reutilization. During the process, Pb was efficiently removed from the hazardous material and nano-Pb particles could be successfully synthesized. The optimum temperature, holding time, system pressure, and argon gas flow rate for the process were 1000 °C, 2–4 h, 500–2000 Pa, and 50–200 ml/min, respectively, and the maximum lead evaporation ratio was 96.8% and the prepared lead nanoparticles dispersed evenly with average diameter range from 4 nm to 34 nm. TCLP results show that the residue glass powder, which was effectively detoxified could be applied for functional materials production.

Acknowledgements

This work was made possible by the financial supports from the National Key Technology R&D Program (2008BAC32B03), the Environmental Public Welfare Project (201009026) and the National Water Pollution Control Program (2009ZX07212-002).

References

[1] M.J. Chen, F.S. Zhang, J.X. Zhu, Effective utilization of waste cathode ray tube glass—crystalline silicotitanate synthesis, J. Hazard. Mater. 182 (2010) 45–49.
[2] F. Mear, P. Yot, M. Cambon, M. Ribes, The characterization of waste cathode-ray tube glass, Waste Manage. 26 (2006) 1468–1476.
[3] P.G. Yot, F.O. Mear, Characterization of lead, barium and strontium leachability from foam glasses elaborated using waste cathode ray-tube glasses, J. Hazard. Mater. 185 (2011) 236–241.
[4] M. Yamashita, A. Wannagon, S. Matsumoto, T. Akai, H. Sugita, Y. Imoto, T. Komai, H. Sakanakura, Leaching behavior of CRT funnel glass, J. Hazard. Mater. 184 (2010) 58–64.
[5] F. Mear, P. Yot, M. Cambon, M. Ribes, The changes in lead silicate glasses induced by the addition of a reducing agent (TiN or SiC), J. Non-Cryst. Solids 351 (2005) 3314–3319.
[6] F.O. Mear, P.G. Yot, A.V. Kolobov, M. Ribes, M.F. Guimon, D. Gonbeau, Local structure around lead, barium and strontium in waste cathode-ray tube glasses, J. Non-Cryst. Solids 353 (2007) 4640–4646.
[7] P.W. Wang, L.P. Zhang, Structural role of lead in lead silicate glasses derived from XPS spectra, J. Non-Cryst. Solids 194 (1996) 129–134.
[8] R. Sasai, H. Kubo, M. Kamiya, H. Itoh, Development of an eco-friendly material recycling process for spent lead glass using a mechanochemical process and Na_2EDTA reagent, Environ. Sci. Technol. 42 (2008) 4159–4164.
[9] A.J. Saterlay, S.J. Wilkins, R.G. Compton, Towards greener disposal of waste cathode ray tubes via ultrasonically enhanced lead leaching, Green Chem. 3 (2001) 149–155.
[10] H. Miyoshi, D.P. Chen, T. Akai, A novel process utilizing subcritical water to remove lead from wasted lead silicate glass, Chem. Lett. 33 (2004) 956–957.
[11] M.A. El-Sayed, Some Interesting properties of metals confined in time and nanometer space of different shapes, Acc. Chem. Res. 34 (2001) 257–264.
[12] M. Martos, J. Morales, L. Sanchez, Lead-based systems as suitable anode materials for Li-ion batteries, Electrochim. Acta 48 (2003) 615–621.
[13] J. An, H.X. Wu, Y.C. Xin, Preparation and research of resin/nano-lead composite for high-energy radiation protection, Eng. Plast. Appl. 32 (2004) 14–17 (in Chinese).
[14] R.S. Li, H. Hao, W.B. Cai, T. Huang, A.S. Yu, Preparation of carbon supported Pd–Pb hollow nanospheres and their electrocatalytic activities for formic acid oxidation, Electrochem. Commun. 12 (2010) 901–904.
[15] M. Veith, J. Frères, P. König, O. Schütt, V. Huch, J. Blin, Nanoscaled Sn and Pb particles aligned in Al2O3 tubes obtained from molecular precursors, Eur. J. Inorg. Chem. 18 (2005) 3699–3710.
[16] S. Michotte, S. Matefi-Tempfli, L. Piraux, 1D-transport properties of single superconducting lead nanowires, Physica C 391 (2003) 369–375.
[17] L.N. Lewis, N. Lewis, Platinum-catalyzed hydrosilylation—colloid formation as the essential step, J. Am. Chem. Soc. 108 (1986) 7228–7231.
[18] K. Torigoe, K. Esumi, Preparation of bimetallic silver–palladium colloids from silver (I) bis (oxalato) palladate(II), Langmuir 9 (1993) 1664–1667.
[19] J.E. Lee, S.M. Oh, D.W. Park, Synthesis of nano-sized Al doped TiO_2 powders using thermal plasma, Thin Solid Films 457 (2004) 230–234.
[20] K.S. Suslick, M. Fang, T. Hyeon, Sonochemical synthesis of iron colloids, J. Am. Chem. Soc. 118 (1996) 11960–11961.
[21] M.T. Reetz, W. Helbig, Size-selective synthesis of nanostructured transition metal clusters, J. Am. Chem. Soc. 116 (1994) 7401–7402.
[22] H. Willwohl, J. Wolfrum, V. Zumbach, P. Albers, K. Seibold, Production and characterization of highly dispersed catalytic active platinum and palladium powders by excimer laser photolysis, J. Phys. Chem. 98 (1994) 2242–2247.
[23] M.Z. Yu, J.Z. Lin, T. Chan, Numerical simulation of nanoparticle synthesis in diffusion flame reactor, Powder Technol. 181 (2008) 9–20.
[24] J. Haidar, Synthesis of Al nanopowders in an anodic arc, Plasma Chem. Plasma Process. 29 (2009) 307–319.
[25] H.M. Lee, Y.R. Uhm, C.K. Rhee, Phase control and characterization of Fe and Fe-oxide nanocrystals synthesized by pulsed wire evaporation method, J. Alloys Compd. 461 (2008) 604–607.
[26] S.H. Lee, S.M. Oh, D.W. Park, Preparation of silver nanopowder by thermal plasma, Mater. Sci. Eng. C 27 (2007) 1286–1290.
[27] P.G. Yot, F.O. Mear, Influence of AlN, TiN and SiC reduction on the structural environment of lead in waste cathode-ray tubes glass: an x-ray absorption spectroscopy study, J. Phys-Condens. Mat. 21 (2009) 104–111.
[28] P.G. Yot, F.O. Mear, Lead extraction from waste funnel cathode-ray tubes glasses by reaction with silicon carbide and titanium nitride, J. Hazard. Mater. 172 (2009) 117–123.
[29] A. Witkowska, J. Rybicki, K. Trzebiatowski, A. Di Cicco, M. Minicucci, Influence of hydrogen reduction on the structure of $PbSiO_3$ glass: an EXAFS study, J. Non-Cryst. Solids 276 (2000) 19–26.
[30] A. Witkowska, J. Rybicki, A. Di Cicco, Structure of partially reduced xPbO $(1-x)SiO_2$ glasses: combined EXAFS and MD study, J. Non-Cryst. Solids 351 (2005) 380–393.
[31] M.J. Chen, F.S. Zhang, J.X. Zhu, Lead recovery and the feasibility of foam production from funnel glass of dismantled cathode ray tube pyrovacuum process, J. Hazard. Mater. 161 (2009) 1109–1113.
[32] C.H. Lee, C.S. Hsi, Recycling of scrap cathode ray tubes, Environ. Sci. Technol. 36 (2002) 69–75.
[33] S. Yamasaki, Digestion method for total element analysis, in: Method of Soil Environmental Analysis, Japanese society of soil science and plant Nutrition, Hakuyusya, Tokyo, 1997, pp. 278–288 (in Japanese).
[34] U.S. EPA, Test Methods for Evaluating Solid Waste, Office of Solid Waste, Washington, DC, 1996.
[35] Y.N. Dai, B. Yang, Vacuum Metallurgy of Nonferrous Metallic Materials, Metallurgical Industry Press, Beijing, 2006 (in Chinese).
[36] Y.J. Liang, Y.C. Che, Inorganics Thermodynamics Manual, Northeastern University Press, Shenyang, 1994 (in Chinese).
[37] B. Giesen, H.R. Orthner, A. Kowalik, P. Roth, On the interaction of coagulation and coalescence during gas-phase synthesis of Fe-nanoparticle agglomerates, Chem. Eng. Technol. 59 (2004) 2201–2211.
[38] T. Swihart Mark, Vapor-phase synthesis of nanoparticles, Curr. Opin. Colloid Interface Sci. 8 (2003) 127–133.
[39] K. Wegner, B. Walker, S. Tsantilis, S.E. Pratsinis, Design of metal nanoparticle synthesis by vapor flow condensation, Chem. Eng. Technol. 57 (2002) 1753–1762.
[40] A. Simchi, R. Ahmadi, S.M.S. Reihani, A. Mahdavi, Kinetics and mechanisms of nanoparticle formation and growth in vapor phase condensation process, Mater. Des. 28 (2007) 850–856.